Articles

Mechanistic Inferences from the Binding of Ligands to LpxC, a Metal-Dependent Deacetylase[†,‡]

Heather A. Gennadios,[§] Douglas A. Whittington,[§,||] Xuechen Li,[⊥] Carol A. Fierke,[#] and David W. Christianson*[,§]

Roy and Diana Vagelos Laboratories, Department of Chemistry, University of Pennsylvania, Philadelphia, Pennsylvania 19104-6323, Department of Chemistry, University of Alberta, W5-15 Edmonton, Alberta, Canada T6G 2G2, and Department of Chemistry, University of Michigan, Ann Arbor, Michigan 48109

Received April 26, 2006; Revised Manuscript Received May 11, 2006

ABSTRACT: The metal-dependent deacetylase LpxC catalyzes the first committed step of lipid A biosynthesis in Gram-negative bacteria. Accordingly, LpxC is an attractive target for the development of inhibitors that may serve as potential new antibiotics for the treatment of Gram-negative bacterial infections. Here, we report the 2.7 Å resolution X-ray crystal structure of LpxC complexed with the substrate analogue inhibitor TU-514 and the 2.0 Å resolution structure of LpxC complexed with imidazole. The X-ray crystal structure of LpxC complexed with TU-514 allows for a detailed examination of the coordination geometry of the catalytic zinc ion and other enzyme−inhibitor interactions in the active site. The hydroxamate group of TU-514 forms a bidentate chelate complex with the zinc ion and makes hydrogen bond interactions with conserved active site residues E78, H265, and T191. The inhibitor C-4 hydroxyl group makes direct hydrogen bond interactions with E197 and H58. Finally, the C-3 myristate moiety of the inhibitor binds in the hydrophobic tunnel of the active site. These intermolecular interactions provide a foundation for understanding structural aspects of enzyme−substrate and enzyme−inhibitor affinity. Comparison of the TU-514 complex with cacodylate and imidazole complexes suggests a possible substrate diphosphate binding site and highlights residues that may stabilize the tetrahedral intermediate and its flanking transition states in catalysis. Evidence of a catalytic zinc ion in the native zinc enzyme coordinated by H79, H238, D242, and two water molecules with square pyramidal geometry is also presented. These results suggest that the native state of this metallohydrolase may contain a pentacoordinate zinc ion, which contrasts with the native states of archetypical zinc hydrolases such as thermolysin and carboxypeptidase A.

The outer leaflet of the outer membrane of a Gram-negative bacterium is composed of lipopolysaccharide (LPS),[1] which serves as a permeability barrier that protects the bacterium against erythromycin and other antibiotics (*1*−*6*). Each LPS molecule contains O-antigen polysaccharide and core oligosaccharide domains covalently attached to lipid A, a glucosamine-based phospholipid that is the immunologically active component of LPS (*4*−*6*). Lipid A is required for the viability of Gram-negative bacteria, and its biosynthesis has accordingly attracted attention as a therapeutic target for the treatment of Gram-negative bacterial infections (*5*−*10*).

The first committed step in lipid A biosynthesis is catalyzed by a metal-dependent deacetylase, UDP-{3-*O*-[(*R*)-3-hydroxymyristoyl]}-*N*-acetylglucosamine deacetylase (LpxC), which hydrolyzes UDP-{3-*O*-[(*R*)-3-hydroxymyristoyl]}-*N*-acetylglucosamine to form acetate and UDP-{3-*O*-[(*R*)-3-hydroxymyristoyl]}glucosamine (*11*−*14*). The three-dimensional structure of LpxC from *Aquifex aeolicus* has been determined by X-ray crystallography (*15*) and NMR spectroscopy (*16*, *17*) and reveals a novel $\alpha + \beta$ fold and the new zinc-binding motif, HKX(L,F)D. In the mechanism first proposed on the basis of the analysis of the X-ray crystal structure (*15*), E78 serves as a general base by abstracting a proton from the zinc-bound water molecule to promote nucleophilic attack at the substrate, and this aspect of the catalytic mechanism has been probed in detailed structural and enzymological studies (*17*−*19*).[2] The results of site-

[†] This work was supported by National Institutes of Health Grants GM49758 (D.W.C.) and GM40602 (C.A.F.).

[‡] The atomic coordinates for LpxC complexed with TU-514 and imidazole have been deposited in the Protein Data Bank as entries 2GO4 and 2GO3, respectively.

* To whom correspondence should be addressed. Telephone: (215) 898-5714. Fax: (215) 573-2201. E-mail: chris@sas.upenn.edu.

[§] University of Pennsylvania.

[||] Current address: Amgen, Inc., One Kendall Square, Bldg. 1000, Cambridge, MA 02139.

[⊥] University of Alberta. Current address: Department of Chemistry and Chemical Biology, Harvard University, 12 Oxford St., Cambridge, MA 02138.

[#] University of Michigan.

[1] Abbreviations: LPS, lipopolysaccharide; TU-514, 1,5-anhydro-2-*C*-(carboxymethyl-*N*-hydroxamide)-2-deoxy-3-*O*-myristoyl-D-glucitol; UDP, uridine 5′-diphosphate; NCS, noncrystallographic symmetry; HEPES, 4-(2-hydroxyethyl)piperazine-1-ethanesulfonic acid; PEG, polyethylene glycol; EXAFS, extended X-ray absorption fine structure.

10.1021/bi060823m CCC: $33.50
Published on Web 06/14/2006

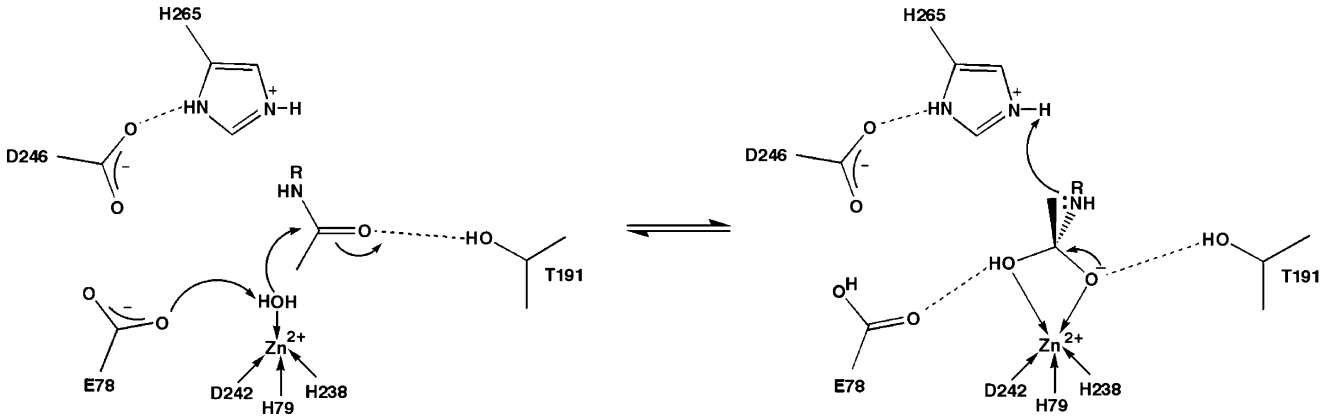

FIGURE 1: Proposed mechanism of LpxC. E78 serves as a general base to abstract a proton from a zinc-bound water molecule, which attacks the substrate carbonyl to form a tetrahedral intermediate stabilized by interactions with zinc and T191. The imidazolium side chain of H265 serves as a general acid and protonates the amine leaving group to facilitate collapse of the tetrahedral intermediate.

directed mutagenesis studies are consistent with this role for E78 in catalysis (*18*, *19*). The oxyanion of the resulting tetrahedral intermediate is stabilized by zinc coordination and hydrogen bonding with T191 based on intermolecular interactions observed in the LpxC−cacodylate and LpxC−palmitate complexes (*19*). Cacodylate and palmitate also hydrogen bond with E78 and H265, implicating these residues in the stabilization of the tetrahedral intermediate and its flanking transition states (*19*), which is consistent with the results of site-directed mutagenesis studies (*18*, *19*) and the pK_a values of ∼6 and ∼8 measured for E78 (*18*, *19*) and H265, respectively (*17*). Site-directed mutagenesis experiments and analysis of the NMR structure of LpxC also implicate K239 as an electrostatic catalyst in the stabilization of the tetrahedral intermediate (*16*, *18*). Although E78 has been considered a potential general acid catalyst for the protonation of the leaving amino group in the collapse of the tetrahedral intermediate (*15*, *18*), analysis of the LpxC−cacodylate complex suggests that H265 is more appropriately positioned to protonate the leaving group (*19*). Accordingly, E78 and H265 may function as a general acid−base catalyst pair (Figure 1) (*19*, *20*).

Recently, the structure of LpxC from *A. aeolicus* complexed with the substrate analogue inhibitor TU-514 [1,5-anhydro-2-*C*-(carboxymethyl-*N*-hydroxamide)-2-deoxy-3-*O*-myristoyl-D-glucitol] (*21*−*23*) has been determined by NMR spectroscopy (*16*, *17*). TU-514 lacks the UDP moiety and the 3-hydroxy group of the myristoyl ester chain of the actual substrate (Figure 2). Additionally, in place of the scissile amide linkage of the substrate, TU-514 contains a hydroxamate "warhead" that targets the catalytic zinc ion. Although the hydroxamate group is a key feature responsible for high-affinity binding of the inhibitor to LpxC, the NMR structure of the enzyme−inhibitor complex does not reveal the characteristic five-membered ring zinc−chelate interaction expected for the inhibitor hydroxamate group; instead, zinc

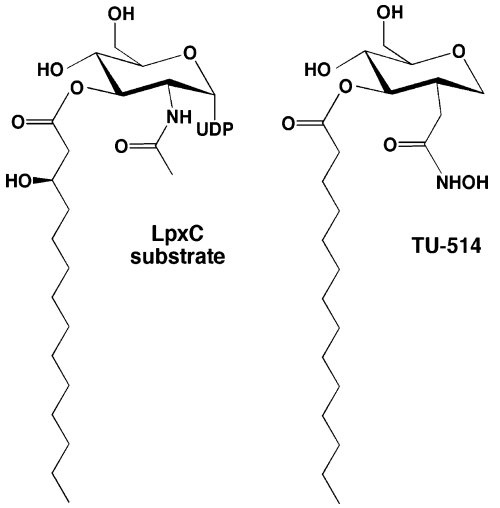

FIGURE 2: Biological substrate of LpxC, UDP-{3-*O*-[(*R*)-3-hydroxymyristoyl]}-*N*-acetylglucosamine, and the substrate analogue inhibitor 1,5-anhydro-2-*C*-(carboxymethyl-*N*-hydroxamide)-2-deoxy-3-*O*-myristoyl-D-glucitol (TU-514; IC_{50} ∼ 7 μM and K_i ∼ 650 nM against LpxC enzymes from *A. aeolicus* and *E. coli*) (*21*, *23*).

coordination is described as being tetracoordinate (*16*). Although the NMR structure of the LpxC−TU-514 complex yields important information regarding other features of inhibitor binding (*16*, *17*), e.g., the binding of the O-3 myristic acid of TU-514 in the active site hydrophobic tunnel [where fatty acid binding is observed in the X-ray crystal structure of the zinc-inhibited enzyme (*15*)], X-ray crystallography is the definitive technique for the examination of precise enzyme−inhibitor zinc coordination and hydrogen bond interactions in the active site.

Here, we report the 2.7 Å resolution X-ray crystal structure of *A. aeolicus* LpxC complexed with TU-514, which reveals a pentacoordinate zinc ion. We also present structural evidence for two zinc-bound water molecules in the structure of wild-type LpxC determined in the presence of 5 mM imidazole. These structures provide key inferences on enzyme−substrate recognition and changes in the zinc coordination polyhedron that may accompany catalysis.

MATERIALS AND METHODS

Determination of the Structure of LpxC Complexed with TU-514. C193A/ΔD284−L294 LpxC from *A. aeolicus*

[2] Here, the numbering system for the well-studied LpxC enzyme from *E. coli* is adapted for the *A. aeolicus* enzyme. On the basis of an alignment performed with Clustal W, important residues conserved between *E. coli* and *A. aeolicus* are as follows: R58 and H58, E78 and E73, H79 and H74, K143 and R137, F161 and F155, T191 and T179, F192 and F180, F194 and F182, E197 and D185, H238 and H226, K239 and K227, D242 and D230, D246 and D234, K262 and R250, and H265 and H253.

(henceforth LpxC) was overexpressed in *Escherichia coli* and purified as described previously (*15*, *24*). Crystallization of the zinc-inhibited enzyme was achieved as previously reported (*19*), and crystals were cross-linked with glutaraldehyde using the technique described by Lusty (*25*), in which LpxC crystals from hanging drops were placed over a microbridge containing a sitting droplet of 2 μL of 25% glutaraldehyde (pH 3). The microbridge rested within a reservoir containing 500 μL of stabilization buffer [100 mM HEPES (pH 7.5), 180 mM NaCl, 16% PEG 3350, and 5 mM $ZnSO_4$]. The cross-linking reaction was allowed to proceed for 45 min, after which the coverslip containing the hanging drop of crystals was placed over a well containing 500 μL of stabilization buffer lacking $ZnSO_4$. An inhibitor buffer solution [100 mM HEPES (pH 7.5), 180 mM NaCl, 16% PEG 3350, 1% glycerol, and 2 mM TU-514] was slowly added to the hanging drop to a final volume of 20 μL, and crystals were equilibrated for 16 h. Crystals were prepared for data collection by cryoprotection with 25% glycerol followed by flash-cooling in liquid nitrogen. Diffraction data were measured to 2.7 Å on beamline F1 at the Cornell High Energy Synchrotron Source (CHESS, Ithaca, NY). Crystals were isomorphous with those of the zinc-inhibited enzyme and belonged to space group $P6_1$ with two monomers in the asymmetric unit and the following unit cell parameters: $a = b = 100.7$ Å, and $c = 121.3$ Å. Data were indexed and merged using HKL2000 (*26*). The structure was determined by the difference Fourier technique. It was evident in the initial electron density maps that the inhibitory zinc ion had been displaced by TU-514, which was coordinated to the catalytic zinc ion (Zn^{2+}_A) with its O-3 myristoyl ester chain extending into the hydrophobic tunnel. Poor electron density for the C-11−C-14 atoms of the myristoyl ester was observed, presumably due to the increasing molecular disorder of the aliphatic tail as it nears the end of the hydrophobic tunnel. Additionally, the C-11−C-14 segment adopts different conformations in monomers A and B to avoid steric clashes in the crystal lattice. Loss of the inhibitory zinc ion, Zn^{2+}_B, was confirmed in anomalous scattering difference maps (data not shown). Iterative cycles of refinement and model building were performed with CNS (*27*) and O (*28*), respectively, to improve the structure as monitored by R_{free}. Restrained noncrystallographic symmetry (NCS) was employed in refinement with the appropriate weights and slightly relaxed as refinement progressed as guided by R_{free}. Atomic coordinates of solvent molecules and TU-514 were added during the last stages of refinement. Data collection and refinement statistics are reported in Table 1.

Determination of the Structure of LpxC Complexed with Imidazole. We first cross-linked crystals of zinc-inhibited LpxC by transferring crystals to a hanging drop containing 10 μL of stabilization buffer [100 mM HEPES (pH 8.0), 180 mM NaCl, 12% PEG 3350, 1% glycerol, and 5 mM $ZnSO_4$] over a well containing 500 μL of stabilizing buffer and 40 μL of 25% glutaraldehyde for approximately 3.5 h. Subsequently, crystals were soaked in stabilizing buffer and 5 mM imidazole for 15 h. Crystals were cryoprotected in 22% glycerol and flash-cooled in liquid nitrogen. Data were collected on beamline X4A at the National Synchrotron Light Source at Brookhaven National Laboratory (Upton, NY). Crystals belonged to space group $P6_1$ with the following unit cell parameters: $a = b = 101.2$ Å, and $c = 122.2$ Å. Data were indexed and merged using HKL2000 (*26*). The structure was determined using the difference Fourier technique. Initial electron density maps showed that the inhibitory zinc ion had been displaced by imidazole. In addition, other imidazole−zinc coordination interactions were evident at the Zn^{2+}_C site, and a fatty acid remnant from heterologous expression in *E. coli* was observed bound in the hydrophobic tunnel. In monomer A, the fatty acid was observed bound in a flipped orientation with its carboxylate headgroup extending from the solvent-exposed end of the tunnel. In monomer B, the fatty acid was observed bound with its carboxylate headgroup extending into the active site, accepting hydrogen bonds from water molecules 292 and 214. Another fatty acid remnant was bound at the interface between the two monomers. Refinement and model building were performed with CNS (*27*) and O (*28*), respectively. With further refinement, the electron density for imidazole at the catalytic zinc ion was interpreted as a 50%-occupied zinc-bound imidazole and a pair of 50%-occupied zinc-bound water molecules. Additional solvent molecules were added during the last stages of refinement. Data collection and refinement statistics are listed in Table 1.

Table 1: Data Collection and Refinement Statistics

	LpxC−TU-514	LpxC−imidazole
resolution range (Å)	50.0−2.7	30−2.0
no. of reflections (measured/unique)	142655/19244	330287/47936
completeness (%) (overall/outer shell)	97.7/97.2	99.8/99.7
R_{merge}[a] (overall/outer shell)	0.069/0.538	0.081/0.319
$\langle I/\sigma \rangle$ (overall/outer shell)	12.6/2.2	21.4/3.9
no. of protein atoms[b]	4298	4298
no. of solvent atoms[b]	64	419
no. of metal ions[b]	5	5
no. of ligand atoms[b]	60	88
no. of reflections used in refinement (work/ free)	16755/846	45400/2393
R/R_{free}[c]	0.210/0.241	0.195/0.235
rms deviations		
bonds (Å)	0.007	0.006
angles (deg)	1.3	1.2
proper dihedral angles (deg)	23.6	23.5
improper dihedral angles (deg)	0.8	0.7

[a] $R_{merge} = \sum|I_j - \langle I_j \rangle|/\sum I_j$, where I_j is the observed intensity for reflection j and $\langle I_j \rangle$ is the average intensity calculated for reflection j from replicate data. [b] Per asymmetric unit. [c] $R = \sum||F_o| - |F_c||/\sum F_o$, where R and R_{free} are calculated using the working and test reflection sets, respectively.

In the figures, molecular structures are illustrated using Bobscript (*29*) and PyMOL (*30*). All least-squares plane calculations for pentacoordinate complexes were made using routines implemented in SHELX (*31*).

RESULTS

LpxC−TU-514 Complex. The transfer of zinc-inhibited LpxC crystals into a solution containing 2 mM TU-514 results in the loss of the inhibitory zinc ion (Zn^{2+}_B) and the binding of TU-514 in the enzyme active site. The structures of enzyme monomers A and B in the asymmetric unit of the crystal are essentially identical, with an rms deviation of 0.019 Å for 267 protein C_α atoms. An electron density map of the LpxC−TU-514 complex is displayed in Figure 3. The structure of the enzyme−inhibitor complex is es-

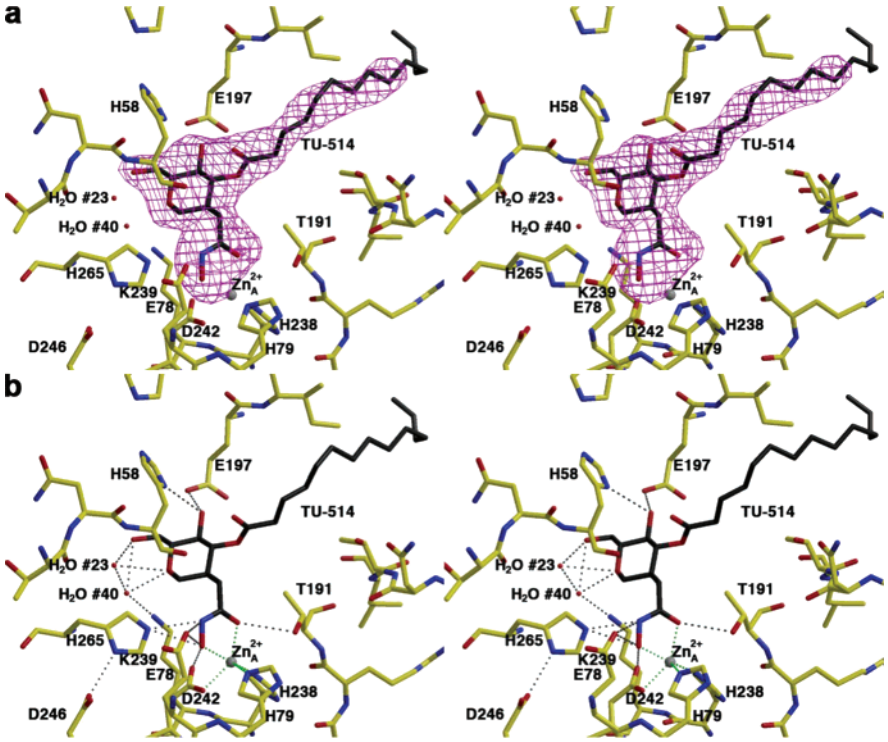

FIGURE 3: (a) Simulated annealing omit electron density map of LpxC complexed with TU-514 (monomer A, contoured at 4σ). Atoms are color-coded as follows: yellow (protein) or black (TU-514) for C, red for O, and blue for N. Zinc appears as a gray sphere; water molecules appear as red spheres. (b) Dashed lines indicate zinc coordination (green) and hydrogen bond (gray) interactions in the LpxC−TU-514 complex.

sentially identical to that of the zinc-inhibited enzyme, with an rms deviation of 0.241 Å for 267 C_α atoms. Both oxygens of the TU-514 hydroxamate group coordinate to the catalytic zinc ion ($Zn^{2+}{}_A$) such that the hydroxamate forms a five-membered ring chelate complex. In addition to $Zn^{2+}{}_A$ coordination, the hydroxamate OH group is within hydrogen bonding distance of E78, H265, and the noncoordinating carboxylate oxygen of the zinc ligand D242. The hydroxamate C═O group accepts a hydrogen bond from T191. It is possible that zinc coordination facilitates ionization of the hydroxamate, as considered by Holmes and Matthews in the first X-ray crystal structures of hydroxamate inhibitors complexed with a zinc enzyme (*32*). The nitrogen atom of the hydroxamate is within hydrogen bonding distance of H265, which is presumed to be a hydrogen bond donor due to its elevated pK_a of ~8 (*17*).

In the LpxC−TU-514 complex, the $Zn^{2+}{}_A$ coordination polyhedron is pentacoordinate with approximate square pyramidal geometry (average deviation of 15° from ideal geometry), with $Zn^{2+}{}_A$ ~0.5 Å out of the least-squares plane defined by H238, D242, and the hydroxamate C═O and OH groups; H79 is the apical ligand. The average trigonality index (τ) is 0.13 for the two enzyme molecules in the asymmetric unit, which corresponds to square pyramidal coordination geometry with very slight trigonalization (τ = 0 for ideal square pyramidal and τ = 0 for ideal trigonal bypyramidal geometry) (*33*). The calculation of τ as an angular structural parameter is analogous to the approach of Muetterties and Guggenberger in using certain shape-determining dihedral angles to characterize the reaction coordinate of square pyramidal ⇔ trigonal bipyramidal ligand rearrangements in Berry pseudorotation processes (*34*). The distances of zinc coordination interactions are recorded in Table 2. In Figure 4, the square pyramidal $Zn^{2+}{}_A$ coordination polyhedron in the LpxC−TU-514 complex is compared with $Zn^{2+}{}_A$ coordination polyhedra observed in other LpxC complexes.

Table 2: $Zn^{2+}{}_A$ Coordination Interactions (Å)[a]

ligand	LpxC−TU-514 complex	LpxC−imidazole complex
H79 Nϵ_2	2.1/2.1	2.1/2.1
H238 Nϵ_2	2.0/2.1	2.1/2.1
D242 Oδ_1	2.2/2.0	2.1/2.1
hydroxamate C═O	2.2/2.1	–
hydroxamate OH	2.0/1.9	–
imidazole N1	–	2.1/2.0
H_2O 416/414	–	2.3/2.3
H_2O 417/415	–	2.3/2.3

[a] Monomer A/B.

The hexose ring of TU-514 is in the chair conformation and makes extensive hydrogen bond interactions in the active site, as expected from the results of chemical mapping experiments (*35*). In monomer A, the hexose ring oxygen accepts hydrogen bonds from water molecules 23 and 40, and these water molecules also hydrogen bond to the C-6 hydroxyl group of the hexose ring. Water molecule 40 is hydrogen bonded to water molecule 23 and K239 (Figure 3). In monomer B, the hexose ring oxygen and the C-6 hydroxyl group are hydrogen bonded to water molecule 41. In both monomers A and B, the C-4 hydroxyl group of the hexose ring hydrogen bonds with E197 and H58. Residue K239 is strictly conserved among 61 currently sequenced LpxC enzymes, but E197 is only partially conserved (16 of 61 as glutamate, 4 of 61 as glutamine, and 41 of 61 as aspartate), and H58 is not conserved (1 of 61; this residue

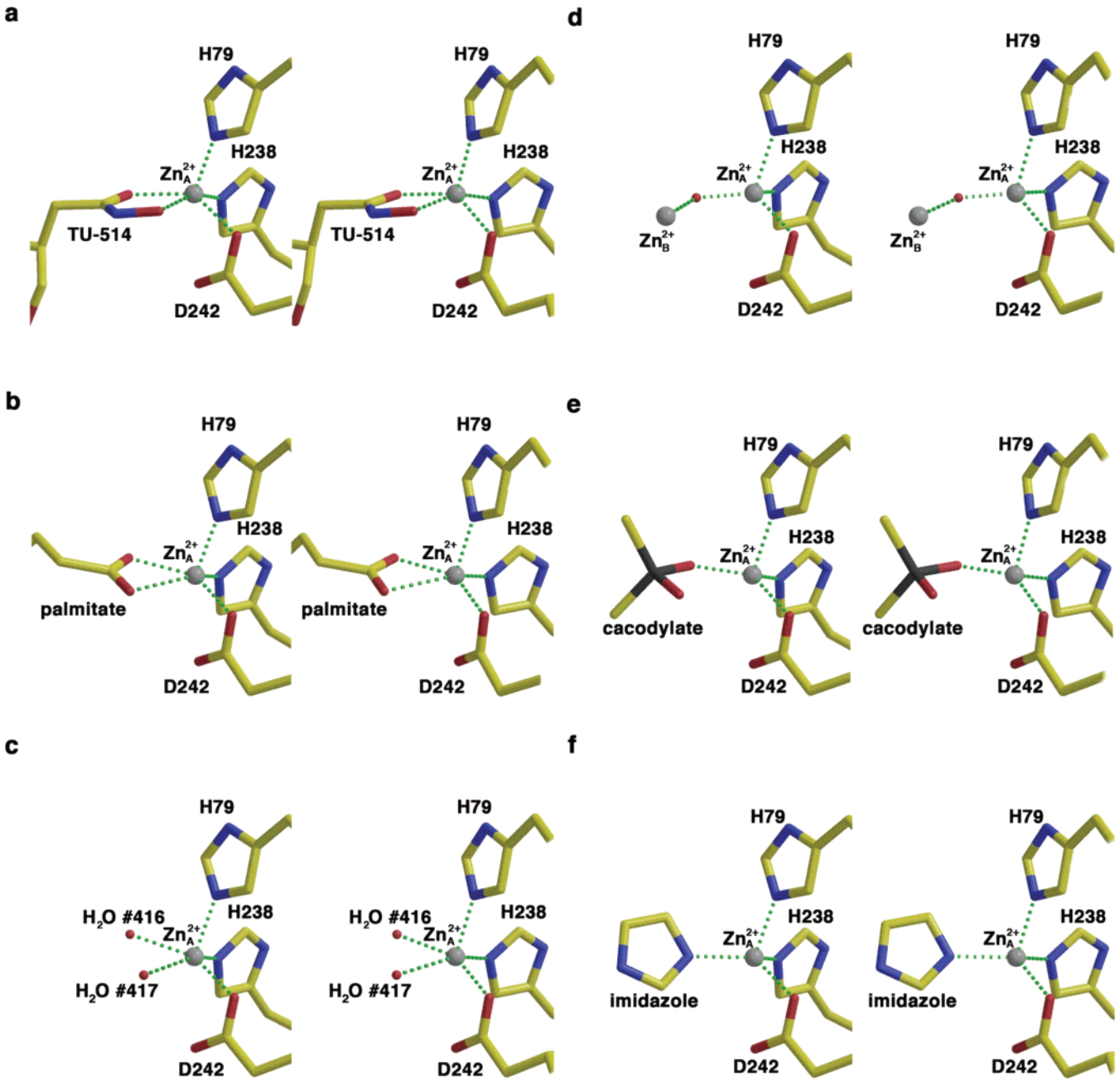

FIGURE 4: Square pyramidal zinc coordination geometry in the (a) LpxC−TU-514 complex, (b) LpxC−palmitate complex (PDB entry 1YH8) (*19*), and (c) LpxC−imidazole complex (50%-occupied zinc-bound water molecules). Tetrahedral zinc coordination geometry in the (d) zinc-inhibited enzyme (PDB entry 1P42) (*15*), (e) LpxC−cacodylate complex (PDB entry 1YHC) (*19*), and (f) LpxC−imidazole complex (zinc-bound imidazole). Atoms are color-coded as follows: yellow for C, red for O, blue for N, and black for As. Zinc appears as a gray sphere; zinc-bound water molecules appear as small red spheres in panel c, and the metal-bridging water molecule appears as a small red sphere in panel d.

usually appears as methionine or leucine and sometimes as arginine).

Although the rms deviations of the TU-514 coordinates between the X-ray crystal structure (monomer A) and the ensemble of NMR structures (PDB entry 1XXE) (*17*) are in the range of 1.45−2.31 Å, the crystal structure of the LpxC−TU-514 complex is in general agreement with the NMR structure (*16*, *17*) with regard to the binding of the O-3 myristate moiety in the active site hydrophobic tunnel. This binding is comparable to that observed for myristate in the crystal structure determination of the zinc-inhibited enzyme (*15*) as well as that observed for binding of palmitate to the native enzyme (*19*). A superposition of the NMR structure ensemble and the X-ray crystal structure is found in Figure 5.

LpxC−Imidazole Complex. The transfer of zinc-inhibited LpxC crystals into a solution containing 5 mM imidazole results in the loss of the inhibitory zinc ion (Zn^{2+}_B) and the binding of imidazole to the catalytic zinc ion (Zn^{2+}_A) and to another zinc ion (Zn^{2+}_C) identified in the zinc-inhibited structure (*15*). Electron density for Zn^{2+}_A-bound imidazole is characterized by additional features that are interpreted as a pair of Zn^{2+}_A-bound water molecules (417/415 and 416/414 in monomer A/B), mutually exclusive with imidazole

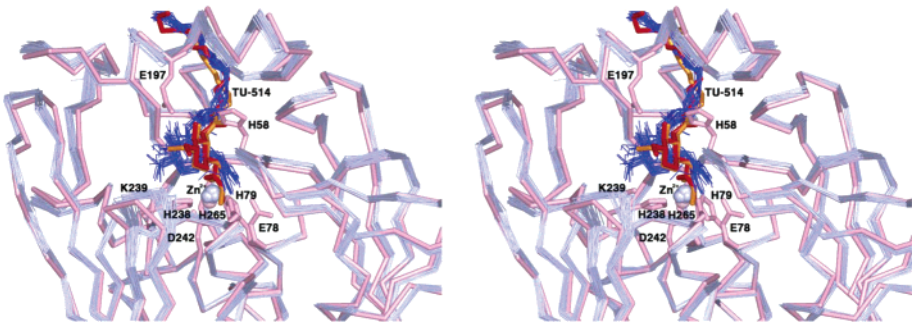

FIGURE 5: Superposition of the X-ray crystal structure of the LpxC−TU-514 complex (monomers A and B) with the ensemble of 25 NMR structures determined by Coggins and colleagues (*17*) (PDB entry 1XXE), oriented so that the viewer is looking directly into the main active site cleft. Pink denotes main chain carbon atoms; zinc appears as a pink sphere, and TU-514 is colored red (monomer A) and orange (monomer B). Selected side chains are indicated and are colored pink. Atoms from the ensemble of 25 NMR strutures are color-coded as follows: light blue for main chain carbon atoms, light blue spheres for Zn^{2+} ions, and blue for TU-514 molecules.

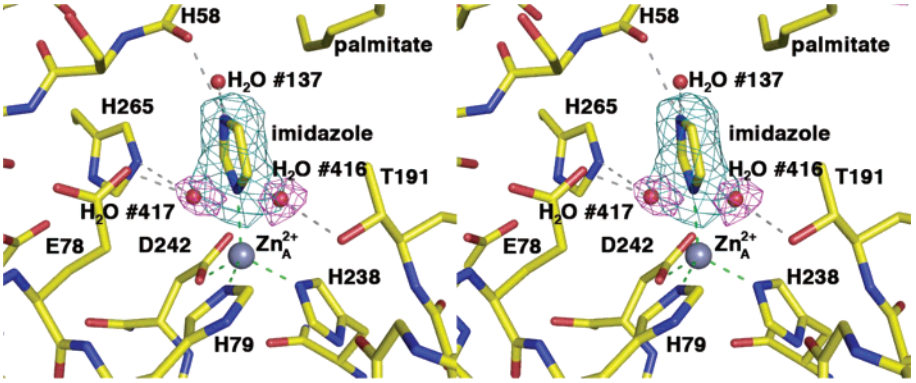

FIGURE 6: Simulated annealing omit electron density maps of LpxC (monomer A) complexed with imidazole (cyan, contoured at 4σ) and water molecules 416 and 417 (magenta, contoured at 4σ). Atoms are color-coded as follows: yellow for C, red for O, and blue for N. Zinc appears as a gray sphere, and water molecules appear as red spheres. Dashed lines indicate zinc coordination (green) and hydrogen bond (gray) interactions.

at 50% occupancy (Figure 6). The pentacoordinate water-bound complex represents the unliganded, native state of LpxC and is similar to that observed for the native states of MshB, a zinc deacetylase from *Mycobacterium tuberculosis* (*36*), and PgdA, a zinc deacetylase from *Streptococcus pneumoniae* (*37*). The structure of the LpxC−imidazole complex is otherwise identical to that of the zinc-inhibited enzyme (*15*), with an rms deviation of 0.249 Å for 267 C_α atoms.

The $Zn^{2+}{}_A$ coordination polyhedron is tetrahedral in the complex with imidazole (average deviation of 9° from ideal geometry). In monomer A, the imidazole N-1 atom coordinates to $Zn^{2+}{}_A$ and the N-3-H group donates a hydrogen bond to the backbone carbonyl of H58. In monomer B, the N-3-H group donates a hydrogen bond to the backbone carbonyl of H58 and also to water molecule 214.

In the unliganded enzyme structure, water molecules 417/415 and 416/414 (monomer A/B) form a pentacoordinate complex with $Zn^{2+}{}_A$ that adopts approximate square pyramidal geometry (average deviation of 16° from ideal geometry) with $Zn^{2+}{}_A$ ~0.4 Å out of the least-squares plane defined by H238, D242, and water molecules 417/415 and 416/414; H79 is the apical ligand. The average trigonality index τ is 0.12 for the two enzyme molecules in the asymmetric unit, which corresponds to very slightly trigonalized square pyramidal coordination geometry (*33*). Water molecule 417/415 is within hydrogen bonding distance of E78 and H265, and water molecule 416/414 is within hydrogen bonding distance of T191. Zinc coordination polyhedra in LpxC complexes are illustrated and compared in Figure 4.

DISCUSSION

Structural Basis of Inhibitor Affinity. The X-ray crystal structure of the LpxC−TU-514 complex provides important information that will aid in the future design of inhibitors capable of targeting enzymes from a broad spectrum of Gram-negative bacteria. To date, it has been demonstrated that TU-514 exhibits modest inhibition against LpxC enzymes from *A. aeolicus* and *E. coli* with IC_{50} values of ~7 μM against each (*21*) and K_i values of ~650 nM against each (*23*). It is notable that apart from a water-mediated hydrogen bond interaction between the hexose ring oxygen of TU-514 and strictly conserved K239, all of the intermolecular hydrogen bond interactions of the hexose ring occur with LpxC residues that are at best only partially conserved across the species. Accordingly, the hexose ring may be dispensable in inhibitor design. In this regard, it is interesting that fatty acid derivatives containing functional groups such as CO_2^-, SO_3^-, and PO_3^{2-}, but completely lacking a hexose ring moiety, exhibit dissociation constants as low as 300 nM against LpxC (*15*). Additionally, a slow-binding LpxC inhibitor lacking the hexose moiety, CHIR-090, exhibits a K_i value of ~1 nM (*23*).

Despite the significant differences between the X-ray crystal structure and the NMR structure of the LpxC−TU-514 complex in the vicinity of the catalytic zinc ion, a feature common to both structures is the insertion of the C-3 myristoyl tail into the conserved, ~15 Å long hydrophobic tunnel. As previously suggested, this may stabilize the

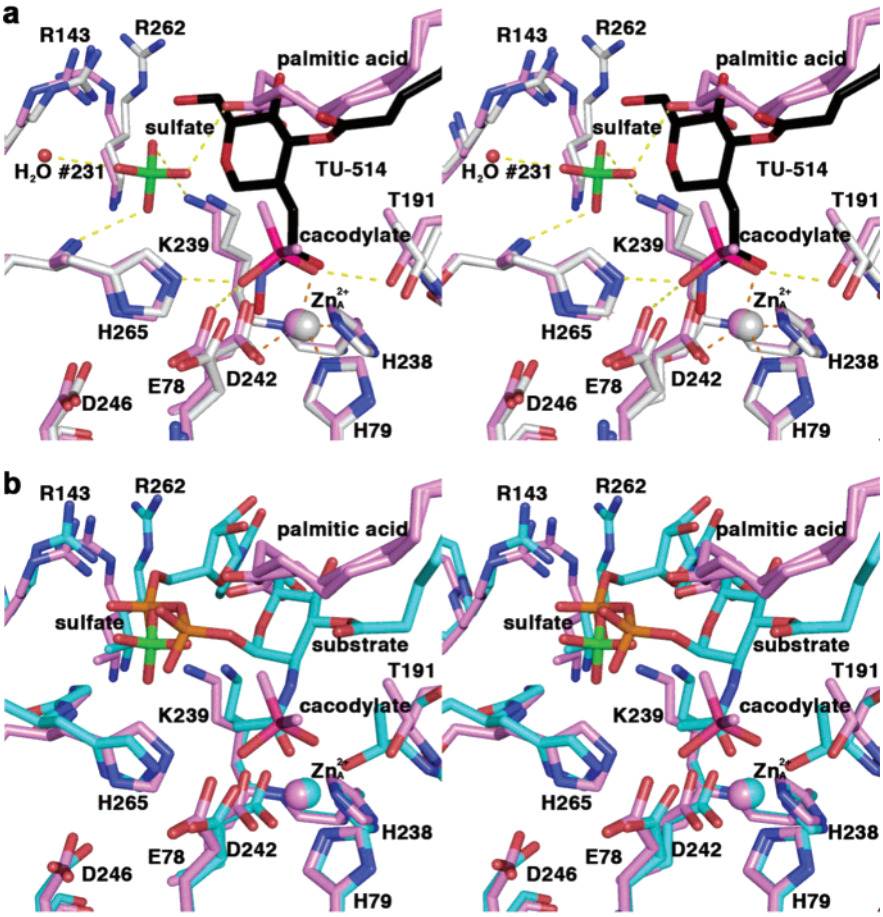

FIGURE 7: (a) Superposition of LpxC−cacodylate (violet) and LpxC−TU-514 (gray; TU-514 colored black) complexes. Hydrogen bond interactions (yellow) and metal coordination interactions (orange) in the LpxC−cacodylate complex are denoted with dashed lines. All non-carbon atoms are color-coded as follows: red for O, blue for N, green for S, and magenta for As. Zinc ions appear as violet (LpxC−cacodylate complex) or gray (LpxC−TU-514 complex) spheres; water molecule 231 appears as a small red sphere. (b) Superposition of the LpxC−cacodylate complex (violet) and a model of the LpxC−substrate complex (cyan). All non-carbon atoms are color-coded as follows: red for O, blue for N, green for S, magenta for As, and orange for P. Zinc ions appear as violet (LpxC−cacodylate complex) or cyan (model of the LpxC−substrate complex) spheres.

conformation of the $\beta\alpha\beta$ subdomain that frames the hydrophobic tunnel and forms one wall of the active site cleft (*15*, *16*). The NMR spectra indicate increased mobility for this region of the protein structure in the absence of inhibitor binding, so the insertion of the C-3 myristoyl tail into the hydrophobic tunnel is likely required to stabilize the active site in the proper conformation for catalysis (*16*). This hypothesis is supported by a more than 5×10^6-fold decrease in activity observed for the catalysis of the deacetylation of UDP-*N*-acetylglucosamine, which lacks a 3-*O*-[(*R*)-3-hydroxymyristoyl] substituent to bind in the hydrophobic tunnel (*24*).

Thus, as first noted by Whittington and colleagues (*15*), two key, minimal components of an LpxC inhibitor are (1) a functional group to coordinate to Zn^{2+}_A and (2) a long hydrophobic moiety to occupy the hydrophobic tunnel. Additional affinity determinants outlined by Coggins and colleagues (*17*) include interactions with the hydrophobic patch defined by F161, F192, and F194 and the "basic patch" defined by K239, R143, R262, and H265. Among the 61 currently sequenced LpxC enzymes, residues within the hydrophobic patch are either fully conserved (F192) or highly conserved (F161 occasionally appears as tyrosine, and F194 occasionally appears as leucine). However, residues R143 and R262 within the basic patch are poorly conserved, with only K239 and H265 appearing as strictly conserved residues. The basic patch is proposed as a possible binding site for the substrate diphosphate group (*17*), and analysis of the X-ray crystal structure of the LpxC−UDP complex suggests that additional intermolecular interactions can be exploited in the basic patch to enhance enzyme−inhibitor affinity (unpublished results).

Inferences on Substrate Binding. The X-ray crystal structures of the LpxC−TU-514 complex and the LpxC−cacodylate complex (*19*) yield important inferences on substrate binding in the active site. The UDP group is an axial substituent of C-1 of the hexose ring of the substrate and is proposed to interact with positively charged residues, such as those in the basic patch (*17*), to stabilize the negatively charged diphosphate group. Interestingly, in the previously reported structure of LpxC complexed with cacodylate (*19*) (PDB entry 1YHC), a sulfate ion binds in the basic patch. This sulfate ion forms an electrostatic interaction with K239 (3.5 Å) and accepts a hydrogen bond from the backbone NH group of H265, the carboxylic acid headgroup of palmitate, and a water molecule. The sulfate ion is positioned approximately 2 Å from the hexose C-1 atom of TU-514 when the structures of the LpxC−TU-514 and LpxC−cacodylate complexes are superimposed (Figure 7a). Indeed, the crystal structure of the LpxC−UDP complex

confirms that the bound sulfate ion mimics the binding of a UDP phosphate group (unpublished results).

Superposition of the LpxC−cacodylate complex with the LpxC−TU-514 complex also provides insight regarding the position and orientation of the tetrahedral intermediate in the proposed catalytic mechanism (*17*−*19*). The arsenic atom of cacodylate is 0.7 Å from the carbonyl carbon of the hydroxamate headgroup of TU-514. The As−O-2 bond closely aligns with the hydroxamate C═O group and may thus represent the position of the substrate C═O group in the enzyme−substrate complex. The structural inferences emanating from the comparison of the two complexes in Figure 7a suggest the model for substrate binding illustrated in Figure 7b, which updates the model first presented by Whittington and colleagues (*15*).

Zinc Coordination Geometry and Catalysis. Both tetrahedral and square pyramidal Zn^{2+}_A coordination geometries are observed in X-ray crystal structures of LpxC complexes, and interconversions between these two geometries may accompany catalysis. The proposed catalytic mechanism involves ionization of a water molecule bound to a tetrahedrally coordinated Zn^{2+}_A with the subsequent formation of an oxyanion intermediate stabilized by Zn^{2+}_A coordination and electrostatic interactions with E78, H265, and T191 (Figure 1) (*17*−*19*). Unexpectedly, the imidazole−LpxC complex provides structural evidence for a native Zn^{2+}_A ion coordinated by H79, H238, D242, and two water molecules with square pyramidal geometry. This could possibly indicate that substrate binding requires the displacement of one zinc-bound water molecule to allow for some degree of substrate C═O···Zn^{2+}_A interaction and the retention of the second zinc-bound water molecule as the catalytic nucleophile. This would be similar to the mechanisms proposed for the zinc deacetylases MshB from *M. tuberculosis* (*36*) and PgdA from *S. pneumoniae* (*37*), both of which contain pentacoordinate zinc ions in their native states.

However, extended X-ray absorption fine structure (EXAFS) spectroscopic studies of LpxC from *A. aeolicus* and *Pseudomonas aeruginosa* suggest a four-coordinate zinc ion and a five-coordinate Co^{2+} ion (*38*), so it seems that the equilibrium between a four- and five-coordinate metal ion in LpxC is sensitive to changes in the protein environment. In fact, the conditions utilized in the EXAFS experiments are quite different from those employed in the X-ray crystallographic studies: EXAFS experiments were performed with protein prepared under low-ionic strength conditions [samples were desalted prior to analysis and stabilized in 25 mM HEPES (pH 7.0), 1.5 mM tris(2-carboxyethyl)phosphine, and 10% glycerol], whereas the crystals of LpxC with two zinc-bound water molecules were prepared under higher-ionic strength conditions and stabilized in 100 mM HEPES (pH 8.0), 180 mM NaCl, 12% PEG 3350, 22% glycerol, 5 mM $ZnSO_4$, and 5 mM imidazole. Differences in protein preparations may contribute to the apparent discrepancy between EXAFS and X-ray crystallography results.

The interesting mechanistic feature highlighted by this work is the fact that the native zinc ion in LpxC has a propensity for pentacoordination with square pyramidal coordination geometry under some conditions, which could modify extant mechanistic proposals (*15*−*20*). The possibility of a pentacoordinate rather than a tetracoordinate catalytic zinc ion in the native state of LpxC is consistent with native pentacoordinate zinc ions in other zinc-dependent bacterial deacetylases (*36*, *37*) and contrasts with the zinc coordination observed in the native states of the archetypical zinc hydrolases thermolysin (*39*) and carboxypeptidase A (*40*). Future structural studies of LpxC will allow us to clarify aspects of Zn^{2+}_A coordination changes in the catalytic mechanism.

ACKNOWLEDGMENT

We thank the Cornell High Energy Synchrotron Source (CHESS) and the National Synchrotron Light Source at Brookhaven National Laboratory (NSLS) for beamline access. Also, we thank Dr. Luigi Di Costanzo for assistance with data collection and Drs. Marjorie Harding and Anthony Addison for helpful scientific discussions.

REFERENCES

1. Vaara, M. (1992) Agents that increase the permeability of the outer membrane, *Microbiol. Rev. 56*, 395−411.
2. Vuorio, R., and Vaara, M. (1992) The lipid A biosynthesis mutation lpxA2 of *Escherichia coli* results in drastic antibiotic supersusceptibility, *Antimicrob. Agents Chemother. 36*, 826−829.
3. Vaara, M. (1993) Outermembrane permeability barrier to azithromycin, clarithromycin, and roxithromycin in Gram-negative enteric bacteria, *Antimicrob. Agents Chemother. 37*, 354−356.
4. Nikaido, H., and Vaara, M. (1985) Molecular basis of bacterial outer membrane permeability, *Microbiol. Rev. 49*, 1−32.
5. Raetz, C. R. H. (1990) Biochemistry of endotoxins, *Annu. Rev. Biochem. 59*, 129−170.
6. Raetz, C. R. H. (1993) Bacterial endotoxins: Extraordinary lipids that activate eukaryotic signal transduction, *J. Bacteriol. 175*, 5745−5753.
7. Onishi, H. R., Pelak, B. A., Gerckens, L. S., Silver, L. L., Kahan, F. M., Chen, M.-H., Patchett, A. A., Galloway, S. M., Hyland, S. A., Anderson, M. S., and Raetz, C. R. H. (1996) Antibacterial agents that inhibit lipid A biosynthesis, *Science 274*, 980−982.
8. Wyckoff, T. J., Raetz, C. R. H., and Jackman, J. E. (1998) Antibacterial and anti-inflammatory agents that target endotoxin, *Trends Microbiol. 6*, 154−159.
9. Vaara, M. (1999) in *Endotoxin in health and disease*, pp 31−32, Marcel Dekker, Inc., New York.
10. Rick, P. D., and Raetz, C. R. H. (1999) in *Endotoxin in health and disease*, pp 283−304, Marcel Dekker, Inc., New York.
11. Anderson, M. S., Bulawa, C. E., and Raetz, C. R. (1985) The biosynthesis of Gram-negative endotoxin. Formation of lipid A precursors from UDP-GlcNAc in extracts of *Escherichia coli*, *J. Biol. Chem. 260*, 15536−15541.
12. Anderson, M. S., Robertson, A. D., Macher, I., and Raetz, C. R. H. (1988) Biosynthesis of lipid A in *Escherichia coli*: Identification of UDP-3-*O*-[(*R*)-3-hydroxymyristoyl]-α-D-glucosamine, *Biochemistry 27*, 1908−1917.
13. Anderson, M. S., Bull, H. G., Galloway, S. M., Kelly, T. M., Mohan, S., Radika, K., and Raetz, C. R. H. (1993) UDP-*N*-acetylglucosamine acyltransferase of *Escherichia coli*. The first step of endotoxin biosynthesis is thermodynamically unfavorable, *J. Biol. Chem. 268*, 19858−19865.
14. Young, K., Silver, L. L., Bramhill, D., Cameron, P., Eveland, S. S., Raetz, C. R. H., Hyland, S. A., and Anderson, M. S. (1995) The envA permeability/cell division gene of *Escherichia coli* encodes the second enzyme of lipid A biosynthesis. UDP-3-*O*-(*R*-3-hydroxymyristoyl)-*N*-acetylglucosamine deacetylase, *J. Biol. Chem. 270*, 30384−30391.
15. Whittington, D. A., Rusche, K. M., Shin, H., Fierke, C. A., and Christianson, D. W. (2003) Crystal structure of LpxC, a zinc-dependent deacetylase essential for endotoxin biosynthesis, *Proc. Natl. Acad. Sci. U.S.A. 100*, 8146−8150.
16. Coggins, B. E., Li, X., McClerrin, A. L., Hindsgaul, O., Raetz, C. R. H., and Zhou, P. (2003) Structure of the LpxC deacetylase with a bound substrate-analog inhibitor, *Nat. Struct. Biol. 10*, 645−651.
17. Coggins, B. E., McClerrin, A. L., Jiang, L., Li, X., Rudolph, J., Hindsgaul, O., Raetz, C. R. H., and Zhou, P. (2005) Refined

solution structure of the LpxC-TU-514 complex and pK_a anlaysis of an active site histidine: Insights into the mechanism and inhibitor design, *Biochemistry 44*, 1114−1126.
18. McClerren, A. L., Zhou, P., Guan, Z., Raetz, C. R. H., and Rudolph, J. (2005) Kinetic analysis of the zinc-dependent deacetylase in the lipid A biosynthetic pathway, *Biochemistry 44*, 1106−1113.
19. Hernick, M., Gennadios, H. A., Whittington, D. A., Rusche, K. M., Christianson, D. W., and Fierke, C. A. (2005) UDP-(3-*O*-((*R*)-3-hydroxymyristoyl))-*N*-acetylglucosamine deacetylase functions through a general acid−base catalyst pair mechanism, *J. Biol. Chem. 280*, 16969−16978.
20. Hernick, M., and Fierke, C. A. (2004) Zinc hydrolases: The mechanisms of zinc-dependent deactylases, *Arch. Biochem. Biophys. 433*, 71−84.
21. Jackman, J. E., Fierke, C. A., Tumey, L. N., Pirrung, M., Uchiyama, T., Tahir, S. H., Hindsgaul, O., and Raetz, C. R. H. (2000) Antibacterial agents that target lipid A biosynthesis in Gram-negative bacteria, *J. Biol. Chem. 275*, 11002−11009.
22. Li, X., Uchiyama, T., Raetz, C. R. H., and Hindsgaul, O. (2003) Synthesis of a carbohydrate-derived hydroxamic acid inhibitor of the bacterial enzyme (LpxC) involved in lipid A biosythesis, *Org. Lett. 5*, 539−541.
23. McClerren, A. L., Endsley, S., Bowman, J. L., Andersen, N. H., Guan, Z., Rudolph, J., and Raetz, C. R. H. (2005) A slow, tight-binding inhibitor of the zinc-dependent deacetylase LpxC of lipid A biosynthesis with antibiotic activity comparable to ciproflaxin, *Biochemistry 44*, 16574−16583.
24. Jackman, J. E., Raetz, C. R. H., and Fierke, C. A. (1999) UDP-(3-*O*-(*R*-3-hydroxymyristoyl))-*N*-acetylglucosamine deacetylase of *Escherichia coli* is a zinc metalloenzyme, *Biochemistry 38*, 1902−1911.
25. Lusty, C. J. (1999) A gentle vapor-diffusion technique for cross-linking of protein crystals for cryocrystallography, *Appl. Crystallogr. 32*, 106−112.
26. Otwinowski, Z., and Minor, W. (1997) Processing of X-ray diffraction data collected in oscillation mode, *Methods Enzymol. 276*, 307−326.
27. Brünger, A. T., Adams, P. D., Clore, G. M., De Lano, W. L., Gros, P., Grosse-Kunstleve, R. W., Jiang, J.-S., Kuszewski, J., Nilges, M., Pannu, N. S., Read, R. J., Rice, L. M., Simonson, T., and Warren, G. L. (1998) Crystallography & NMR system: A new software suite for macromolecular structure determination, *Acta Crystallogr. D54*, 905−921.
28. Jones, T. A., Zou, J. Y., Cowan, S. W., and Kjeldjaard, M. (1991) Improved methods for building protein models in electron density maps and the location of errors in these models, *Acta Crystallogr. A47*, 110−119.
29. Esnouf, R. M. (1997) An extensively modified version of MOLSCRIPT that includes greatly enhanced coloring capabilities, *J. Mol. Graphics Modell. 15*, 132−134, 112−113.
30. DeLano, W. L. (2002) *The PyMOL molecular graphics system*, DeLano Scientific, San Carlos, CA.
31. Sheldrick, G. M., and Schneider, T. R. (1997) SHELXL: High-resolution refinement, *Methods Enzymol. 277*, 319−343.
32. Holmes, M. A., and Matthews, B. W. (1981) Binding of hydroxamic acid inhibitors to crystalline thermolysin suggests a pentacoordinate zinc intermediate in catalysis, *Biochemistry 20*, 6912−6920.
33. Addison, A. W., Rao, T. N., Reedijk, J., van Rijn, J., and Verschoor, G. C. (1984) Synthesis, structure, and spectroscopic properties of copper(II) compounds containing nitrogen-sulphur donor ligands: The crystal and molecular structure of aqua[1,7-bis(*N*-methylbenzimidazol-2′-yl)-2,6-dithiaheptane]copper(II) perchlorate, *J. Chem. Soc., Dalton Trans.*, 1349−1356.
34. Muetterties, E. L., and Guggenberger, L. J. (1974) Idealized polytopal forms. Description of real molecules referenced to idealized polygons or polyhedra in geometric reaction path form, *J. Am. Chem. Soc. 96*, 1748−1756.
35. Li, X., McClerren, A. L., Raetz, C. R. H., and Hindsgaul, O. (2005) Mapping the active site of the bacterial enzyme LpxC using novel carbohydrate-based hydroxamic acid inhibitors, *J. Carbohydr. Chem. 24*, 583−609.
36. Maynes, J. T., Garen, C., Cherney, M. M., Newton, G., Arad, D., Av-Gay, Y., Fahey, R. C., and James, M. N. G. (2003) The crystal structure of 1-D-myo-inosityl-2-acetamido-2-deoxy-α-D-gucopyranoside deacetylase (MshB) from *Mycobacterium tuberculosis* reveals a zinc hydrolase with a lactate dehydrogenase fold, *J. Biol. Chem. 278*, 47166−47170.
37. Blair, D. E., Schuttelkopf, A. W., McRae, J. I., and van Aalten, D. M. F. (2005) Structure and metal-dependent mechanism of peptidoglycan deactylase, a streptococcal virulence factor, *Proc. Natl. Acad. Sci. U.S.A. 102*, 15429−15434.
38. McClure, C. P., Rusche, K. M., Peariso, K., Jackman, J. E., Fierke, C. A., and Penner-Hahn, J. E. (2003) EXAFS studies of the zinc sites of UDP-(3-*O*-acyl)-*N*-acetylglucosamine deacetylase (LpxC), *J. Inorg. Biochem. 94*, 78−85.
39. Matthews, B. W. (1988) Structural basis of the action of thermolysin and related zinc peptidases, *Acc. Chem. Res. 21*, 333−340.
40. Christianson, D. W., and Lipscomb, W. N. (1989) Carboxypeptidase A, *Acc. Chem. Res. 22*, 62−69.

BI060823M